

# The cooperative Ru(4d)-Ho(4f) magnetic orderings and phase coexistence in the 6H-perovskite Ba<sub>3</sub>HoRu<sub>2</sub>O<sub>9</sub>

T. Basu<sup>1,2</sup>, V. Caignaert<sup>2</sup>, F. Damay<sup>3</sup>, T.W. Heitmann<sup>4</sup>, B. Raveau<sup>2</sup>, X. Ke<sup>1</sup>

<sup>1</sup>*Department of Physics and Astronomy, Michigan State University, East Lansing, MI 48824, USA*

<sup>2</sup>*Laboratoire CRISMAT, UMR 6508 du CNRS et de l'Ensicaen, 6 Bd Marechal Juin, 14050 Caen, France*

<sup>3</sup>*Laboratoire Léon Brillouin, Grenoble, France*

<sup>4</sup>*Missouri Research Reactor, University of Missouri, Columbia, Missouri 65211, USA*

We report cooperative magnetic orderings in a 6H-perovskite multiferroic system, Ba<sub>3</sub>HoRu<sub>2</sub>O<sub>9</sub>, via comprehensive neutron powder diffraction measurements. This system undergoes long-range antiferromagnetic ordering at  $T_{N1} \sim 50$  K with a propagation wave vector of  $\mathbf{K}_1 = (0.5 \ 0 \ 0)$ , a transition temperature much higher than the previously reported one at  $\sim 10$  K ( $T_{N2}$ ). Both Ru and Ho-moments order simultaneously below  $T_{N1}$ , followed by spin-reorientations at lower temperatures, demonstrating strong Ru(4d)-Ho(4f) magnetic correlation. Below  $T_{N1}$  another magnetic phase with a propagation wave vector  $\mathbf{K}_2 = (0.25 \ 0.25 \ 0)$  emerges and coexists with the one associated with  $\mathbf{K}_1$ , which is rarely observed and suggests complex magnetism due to phase competition in the magnetic ground state.

The electron and magnetic correlation of  $d$  and  $f$  electrons has been a core research topic in condensed matter physics, and it plays a decisive role in determining materials properties, such as unconventional superconductivity, metal-insulator transition, magnetoresistance, multiferroicity, as well as a rich variety of magnetic orderings. Particularly, the strong  $d$ - $f$  magnetic correlations with competing magnetic interactions often give further interesting properties. For instance, the compounds containing magnetic rare-earth ( $R$ )-ions and transition-metal (TM) ions, e.g.  $RMnO_3$ ,<sup>1</sup>  $RMn_2O_5$ ,<sup>1-3</sup>  $R_2BaNiO_5$ <sup>4,5</sup> undergo simultaneous ordering of TM and  $R$ -moments due to  $3d$ - $4f$  magnetic correlation, exhibiting intriguing multiferroicity / strong magnetoelectric coupling.

While there have been extensive studies on the materials exhibiting  $3d$ - $4f$  coupling in recent years, much fewer reports in literature exist on materials composed of both heavy  $R$  and  $4d$  TM ions which could potentially possess strong  $4d$ - $4f$  coupling,<sup>6,7</sup> specifically considering the fact that  $4d/5d$  electron orbitals are of special interest due to their compelling effects of large spin-orbit coupling and extended  $d$ -orbitals. The fascinating pyrochlore ruthenates  $R_2Ru_2O_7$  exhibit Ru<sup>+4</sup>-ordering at high temperature followed by the ordering of rare-earth ions at lower temperature induced by the  $4d$ - $4f$  coupling.<sup>8-10</sup> However, unlike other  $R$ - members, the magnetic ordering of Er and Ru in  $Er_2Ru_2O_7$  is still ambiguous, where effects of strong magnetic anisotropy and crystal-field effect are speculated.<sup>11,12</sup> The double perovskites  $A_2RRuO_6$  ( $A$ =Sr, Ba) exhibit successive

magnetic ordering of  $\text{Ru}^{+5}$  at high temperature followed by  $R$ -ordering at lower temperature for  $R=\text{Ho, Er}$ , whereas, simultaneous magnetic ordering is observed for  $R=\text{Nd}$  and  $\text{Dy}$ .<sup>13–15</sup> On other hand, only one magnetic anomaly is reported for  $\text{Ba}_4\text{RRu}_3\text{O}_{12}$  system where the role of  $\text{Ru}^{4+}/\text{Ru}^{5+}$  and  $R^{3+}$  ions remains unclear.<sup>16</sup> Therefore, the  $d$ - $f$  magnetic correlation is always intriguing for different  $R$ -ions not only for compounds in the same family but also for systems with distinct crystal structures / space groups. Another system of current interest is 6H-perovskite  $\text{Ba}_3\text{BB}'_2\text{O}_9$  ( $B=3d$  transition metal/  $\text{Sr}/\text{Ca}/\text{Na}/$  Lanthanides,  $B'=4d/5d$  metal like  $\text{Ru, Nb, Sb, Ir}$ ), which exhibits versatile exotic properties depending on the nature of  $B$  and  $B'$  ions, such as, dimer system, geometrical frustration, quantum spin-liquid, charge-ordering, unusual valence state, multiferroicity, etc.<sup>17–26</sup>

The system  $\text{Ba}_3\text{RRu}_2\text{O}_9$ , crystallizing in 6H-perovskite structure, consists of  $\text{Ru}_2\text{O}_9$  dimers (face-sharing  $\text{RuO}_6$ -octahedra) which are interconnected by corner-sharing  $\text{MO}_6$  octahedra and possess an average valence state of 4.5 of  $\text{Ru}$ -ion when  $R = R^{3+}$ . Recently, we have reported magnetodielectric (MD) coupling for  $\text{Ba}_3\text{RRu}_2\text{O}_9$ , which is significantly enhanced for heavier rare-earth member  $\text{Ba}_3\text{HoRu}_2\text{O}_9$ .<sup>25,27</sup> Such an enhanced MD coupling and the emergent ferroelectricity in  $\text{Ba}_3\text{HoRu}_2\text{O}_9$  were speculated to arise from stronger  $4d$ - $4f$  magnetic correlation between  $\text{Ru}$  and heavy  $R$ -ions.<sup>25</sup> The light rare-earth compound  $\text{Ba}_3\text{NdRu}_2\text{O}_9$  exhibits a ferromagnetic ordering of  $\text{Nd}$ -moments at  $T_c \sim 24$  K, followed by an antiferromagnetic (AFM) ordering of  $\text{Ru}_2\text{O}_9$  dimer  $\sim 18$  K and canted AFM ordering of  $\text{Nd} \sim 17$  K.<sup>20,28</sup> In contrast, the heavy-rare-earth members ( $R=\text{Tb, Gd, Ho, Er, etc}$ ) undergo AFM ordering at low temperature  $\sim 10$  K, which is ascribed to the ordering of rare-earth ions, without any further magnetic ordering down to 2 K.<sup>29</sup> Until now, there is no report of a detailed magnetic structure of this  $\text{Ba}_3\text{RRu}_2\text{O}_9$  system for any heavy-rare-earth member in this series, which is warranted in order to confirm the speculation of strong  $4d$ - $4f$  magnetic correlation for heavy  $R$ -members.

In this Rapid Communication, via comprehensive neutron powder diffraction measurements, we report simultaneous magnetic ordering of  $\text{Ru}^{4+}/\text{Ru}^{5+}$  and  $\text{Ho}^{+3}$  moments in  $\text{Ba}_3\text{HoRu}_2\text{O}_9$  at  $T_{N1} \sim 50$  K, which is ascribed to strong  $4d$ - $4f$  magnetic correlation. A rare phase-co-existence of two different magnetic structure is revealed below  $T_{N2} \sim 10$  K, arising from competing exchange interactions.

High quality  $\text{Ba}_3\text{HoRu}_2\text{O}_9$  polycrystalline samples were synthesized using solid state chemistry method as described in our earlier report.<sup>25</sup> Magnetic susceptibility measurements were conducted using Superconducting Quantum Interference Device (SQUID) magnetometer, and heat capacity measurements were done using Physical Properties Measurements System (PPMS), both produced from Quantum Design. Neutron powder diffraction measurements were carried out using a two-axis-diffractometer G4.1 with an incident neutron wavelength of  $2.425 \text{ \AA}$  in LLB, France and a triple-axis spectrometer (TRIAX) with incident neutron wavelength of  $2.359 \text{ \AA}$  at the University of Missouri Research Reactor. The magnetic structure was resolved using Fullprof and SARAh program.<sup>30,31</sup>

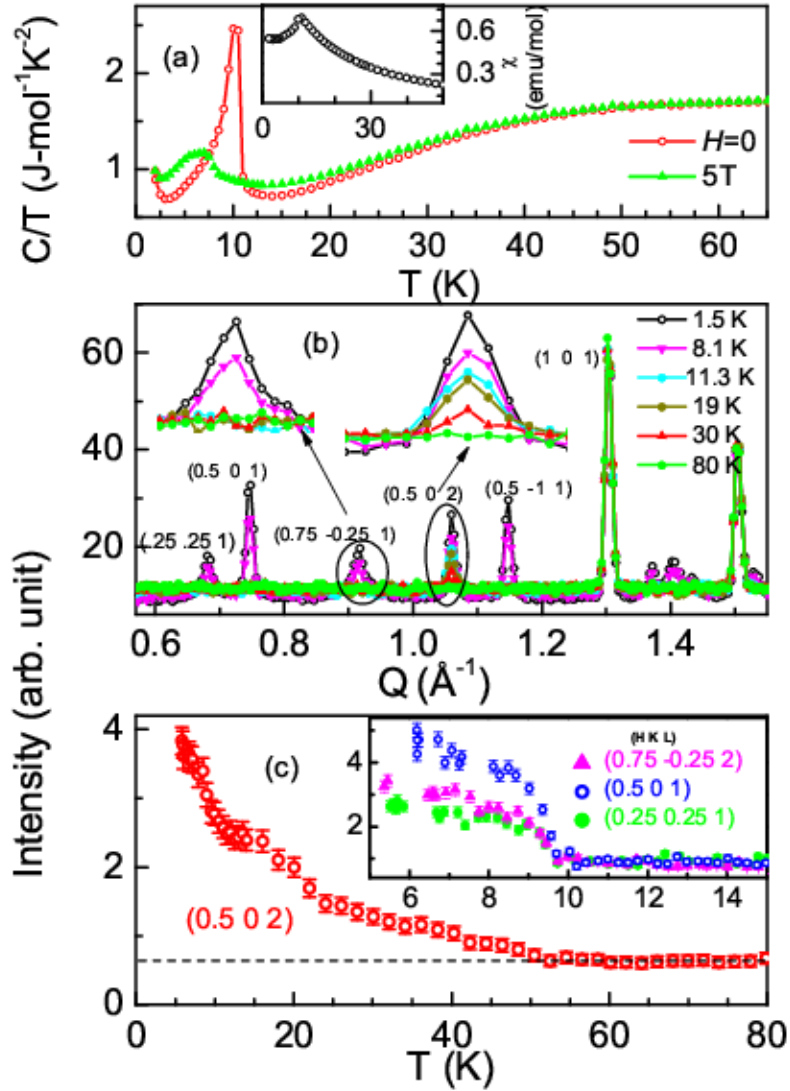


**Fig. 1:** (a) Heat Capacity as a function of temperature measured at  $H = 0$  and 5 T. Inset of (a) shows the magnetic susceptibility as a function of temperature measured at  $H = 1$  T. (b) Powder neutron diffraction pattern collected at different temperatures from 1.5-80 K in low  $Q$ -region. Selective magnetic Bragg peaks are indexed, as described in the text, and the insets show the expanded views. (c) Magnetic Bragg peak intensity of  $(0.5\ 0\ 2)$  plotted as function of temperature measured at zero field. The inset shows the ordering parameter measurements of  $(0.75\ -0.25\ 1)$ ,  $(0.5\ 0\ 1)$  and  $(0.25\ 0.25\ 1)$  magnetic Bragg peaks.

The inset of Fig.1(a) shows the temperature dependence of dc magnetic susceptibility  $\chi$  measured in the presence of 1T magnetic field. The drop in  $\chi$  below 10 K (assigned as  $T_{N2}$ ) indicates an antiferromagnetic (AFM) phase transition, which agrees well with the previous reports.<sup>25,29</sup> The inverse susceptibility (Fig. S1 in Supplemental Material (SM))<sup>32</sup> deviates from linearity (Curie-

Weiss behavior) below  $\sim 100$  K, implying the presence of (short-range) magnetic correlation in this system far above  $T_{N2}$ . The obtained effective moment ( $\mu_{\text{eff}}$ ) and Weiss ( $\Theta_p$ ) temperature, from Curie-Weiss fit between 250-400 K, is  $10.8 \mu_B$  and  $-28$  K, respectively. Considering the full moment of  $\text{Ho}^{+3}$  ( $10.6 \mu_B$ ), the effective moment of Ru ( $1.4 \mu_B$ ) is significantly reduced compare to its theoretical value ( $2.4 \mu_B$ ) of spin-only moment ( $S=1$  for  $\text{Ru}^{+4}$  and  $S=3/2$  for  $\text{Ru}^{+5}$ ). However, short-range magnetic correlations may exist even at very high temperature in this dimmer system, thereby, a true paramagnetic region could not be obtained which could include errors in fitting results.

Figure 1(a) presents the specific heat divided by temperature ( $C/T$ ) in the presence of  $H = 0$  and 5 T dc magnetic field as a function of temperature. The  $C/T$  is nearly constant down to 50 K from high temperature (also see Fig. S1 in SM)<sup>32</sup>, then slowly decreases with lowering the temperature till around 13 K, followed by a  $\lambda$ -shape anomaly around 10 K (Fig. 1a) in the absence of magnetic field, which confirms the long-range magnetic ordering at  $T_{N2}$ . In the presence of 5 T magnetic field, the feature at  $T_{N2}$  shifts to lower temperature ( $\sim 8$  K), consistent with the AFM nature of this system. Interestingly, one can see that the curve measured at  $H = 0$  and 5 T starts to bifurcate below  $\sim 45$  K, further suggesting the presence of magnetic-correlation at much higher temperature compared to  $T_{N2}$ .

In order to have a better understanding of the magnetic ordering of  $\text{Ba}_3\text{HoRu}_2\text{O}_9$ , we have performed neutron power diffraction measurements. Figure 1(b) shows the diffraction intensity as a function of momentum transfer  $Q$  measured at several temperatures ranging from 1.5 to 80 K. The insets present an expanded view at  $Q = 0.93$  and  $1.07 \text{ \AA}^{-1}$ . There are several important features worth pointing out. i) There is no change of nuclear Bragg peaks (also see Fig. S2 in SM)<sup>32</sup> at all temperatures measured, which indicates no structural phase transition down to 1.5 K. ii) Below  $T_{N2}$ , for instance at  $T = 8.1$  K and 1.5 K, there are extra peaks showing up at  $Q = 1.07, 0.93, 0.75$  and  $0.69 \text{ \AA}^{-1}$  compared to the data measured at  $T = 80$  K, indicating their magnetic nature and as to be discussed next, the wave vectors associated with these  $Q$  values are  $(0.5 \ 0 \ 2)$ ,  $(0.75 \ -0.25 \ 1)$ ,  $(0.5 \ 0 \ 1)$ , and  $(0.25 \ 0.25 \ 1)$  respectively, iii) Intriguingly, as shown in the inset of Fig. 1(b), the magnetic Bragg peak at  $Q = 1.07 \text{ \AA}^{-1}$  persists even above  $T_{N2}$ , for instance, at  $T = 11.3$  K, 19 K, and 30 K, while magnetic Bragg peaks at other  $Q$  values disappear. This suggests the presence of another magnetic ordering existing at between 30 K to 80 K, which is far above the previously reported magnetic transition at  $\sim 10$  K ( $T_{N2}$ ). To obtain magnetic ordering temperatures, Figure 1(c) and its inset presents the temperature dependence of scattering intensities measured at aforementioned four  $Q$  values. In contrast to other magnetic Bragg peaks whose intensity drops to the background signal at  $T_{N2}$ , the Bragg peak intensity of  $(0.5 \ 0 \ 2)$  peak sharply decreases when increasing temperature from 2 K (Fig.1c), become nearly constant around  $T_{N2}$ , followed by a gradual drop above 15 K until it reaches the background signal around 50 K ( $T_{N1}$ ). These features clearly indicate that the system undergoes two magnetic phase transitions, one at  $T_{N1} \sim 50$  K and the other at  $T_{N2} \sim 10$  K.

Rietveld refinement of the neutron diffraction data measured at several temperatures using Sarah and Fullprof program are presented in Fig. 2. The details of irreducible representation analysis for magnetic Rietveld refinement are discussed in SM<sup>32</sup>. The Wyckoff positions of Ho and Ru are 2a and 4f, respectively. The atom Ho has two inequivalent positions (0 0 0) and (0 0 0.5), and Ru has four equivalent positions (1/3 2/3 0.16164), (2/3 1/3 0.66164), (2/3 1/3 -0.16164), (1/3 2/3 0.33836). The possible propagation ( $\mathbf{K}$ )-vectors associated with this space group are listed in Table-S1 in the supplementary material. We identify the magnetic propagation vector of the neutron diffraction measured at 30 K and 11.3 K (Fig. 2b and 2c) to be  $\mathbf{K}_1 = (0.5 \ 0 \ 0)$ . Considering the space group P6<sub>3</sub>/mmc and  $\mathbf{K}_1 = (0.5 \ 0 \ 0)$ , there are 4-irreducible representations associated with Ho atom, represented by  $\Gamma_{\text{mag}}(\text{Ho}) = 1\Gamma_1^1 + 0\Gamma_2^1 + 2\Gamma_3^1 + 0\Gamma_4^1 + 1\Gamma_5^1 + 0\Gamma_6^1 + 2\Gamma_7^1 + 0\Gamma_8^1$  and 8-irreducible representation associated with Ru atom, represented by  $\Gamma_{\text{mag}}(\text{Ru}) = 1\Gamma_1^1 + 2\Gamma_2^1 + 2\Gamma_3^1 + 1\Gamma_4^1 + 1\Gamma_5^1 + 2\Gamma_6^1 + 2\Gamma_7^1 + 1\Gamma_8^1$  (see Table S2 and S3). As both Ru and Ho-atoms have ordered magnetic moments, their irreducible representations should contain any of the combinations of  $\Gamma_1$ ,  $\Gamma_3$ ,  $\Gamma_5$  and  $\Gamma_7$ . Other  $\Gamma$ -representations do not produce the magnetic peak. Among these four representations,  $\Gamma_7$ -model gives the best fit. Below  $T_{N2}$  we find that the propagation of the magnetic Bragg peaks can be indexed with a propagation vectors of  $\mathbf{K}_1 = (0.5 \ 0 \ 0)$  and  $\mathbf{K}_2 = (0.25 \ 0.25 \ 0)$ , indicating that two different magnetic phases coexist. Fig. 2d shows the neutron scattering data measured at  $T = 8.1$  K and the refinement results. Considering the space group P6<sub>3</sub>/mmc and  $\mathbf{K}_2 = (0.25 \ 0.25 \ 0)$ , there are 4-irreducible representations associated with Ho atom represented by  $\Gamma_{\text{mag}}(\text{Ho}) = 1\Gamma_1^1 + 1\Gamma_2^1 + 2\Gamma_3^1 + 2\Gamma_4^1$ , and there are 4-irreducible representations associated with Ru atom, represented by  $\Gamma_{\text{mag}}(\text{Ru}) = 3\Gamma_1^1 + 3\Gamma_2^1 + 3\Gamma_3^1 + 3\Gamma_4^1$  (see Table S4 and S5). We find that a combination of  $\Gamma_1$  (for  $\mathbf{K}_2 = (0.25 \ 0.25 \ 0)$ ) and  $\Gamma_7$  (for  $\mathbf{K}_1 = (0.5 \ 0 \ 0)$ ) models gives the best refinement result below  $T_{N2}$ . The Rietveld refinement for 1.5 K data are shown in Figure S2.

The nuclear scattering data at 80 K (Fig. 2a) is well fitted with the space group P6<sub>3</sub>/mmc within the instrumental resolution, which affirms the high crystalline quality of the sample. The neutron scattering data for  $T_{N1} < T < T_{N2}$  (see at  $T = 30$  K and 11.3 K in Fig. 2b and 2c) is well modeled with space group P6<sub>3</sub>/mmc and a wave vector  $\mathbf{K}_1 = (0.5 \ 0 \ 0)$  with an irreducible representation  $\Gamma_7$ . We found that the magnetic peak profile is best modeled only when both Ho and Ru-atoms have non-zero magnetic moment. However, we have tried different possibilities, i) one with fixing magnetic moment of Ho equal to zero and refining the magnetic moment with Ru-atom only (Case-I), and ii) another with fixing the magnetic moment of Ru what is obtained in Case-I (Or, restricted to theoretical value) and then refine the magnetic moments of Ho, iii) the 3<sup>rd</sup> one is refining both the magnetic moments on Ru and Ho-atom. The three cases of the refinement are depicted in Fig.3 for  $T = 11.3$  K. The case-I (Fig. 3-a) gives the worse fitting of the magnetic reflection of (0.5 0 1) compared to that of case-II (Fig. 3-b) and case-III (Fig. 3-a). The magnetic moment of Ru obtained from case-I is  $\sim 2.4 \ \mu_B$  which is equal to the theoretical saturation moment considering spin-only value but much higher than experimentally obtained Ru-moment from magnetic susceptibility. Case-III is slightly better fitted compared to that of case-II. We observe the similar behavior for all other temperatures for  $T_{N2} < T < T_{N1}$  (not shown here). Therefore, these results confirm the

simultaneous ordering of Ru and Ho-moments. Further, we elaborate all these possibilities below  $T_{N2}$ . One argument could be that the Ru-moments order at higher temperature below  $T_{N1}$ , followed by another magnetic structure associated with Ho-moments. If we consider the first case, then Ru-moment at 11.3 K is already saturated (as obtained from refinement in case-I and case-II), therefore, we fix the theoretical value of Ru-moments ( $2.4 \mu_B$ ) and refine the magnetic structure by varying Ho-moment at 8.1 K (see Fig. 3-d). Not only the magnetic reflection  $(0.5 \ 0 \ 1)$  is badly fitted, but another magnetic reflection, which is associated with propagation vector  $\mathbf{K}_1$ ,  $(0.5 \ -1 \ 1)$ , gives negligible intensity in this modeling compared to that of experimentally obtained value. Whereas, the latter case, that is, refinement on both Ho and Ru-moments, gives nearly exact fitting to all the magnetic reflections associated with  $\mathbf{K}_1$  (see Fig. 3-e). Thereby, as discussed in the main manuscript, the neutron data at  $T_{N2} < T < T_{N1}$  are best modeled with magnetic ordering of both Ru and Ho. The obtained Ho and Ru magnetic moments are tabulated in Table-I.

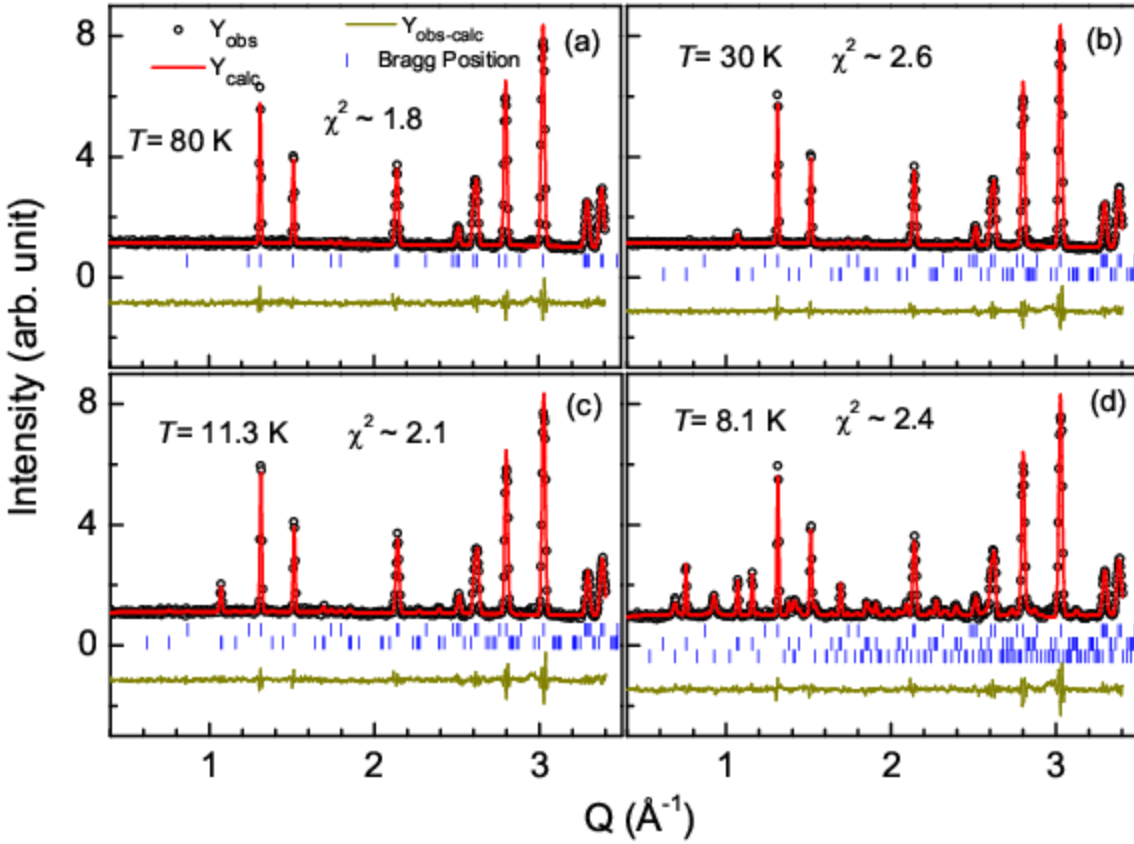


**Fig. 2:** Powder neutron diffraction pattern collected at  $T= 80$  K (a),  $30$  K (b),  $11.3$  K (c) and  $8.1$  K (d) in zero magnetic field. The open black circle represents the experimental data, while the red solid line shows the Rietveld fitting. The vertical bars display the Bragg peak positions. The upper vertical lines represent Bragg peaks of crystal structure of  $\text{Ba}_3\text{HoRu}_2\text{O}_9$ , the next lower vertical lines represent magnetic Bragg peaks associated with  $\mathbf{K}_1 = (0.5 \ 0 \ 0)$  (for (b), (c), and (d)); and lowest vertical line in (d) represents magnetic Bragg peaks associated with  $\mathbf{K}_2 = (0.25 \ 0.25 \ 0)$ . The

continuous dark yellow at the bottom of the figure shows the difference between the experimental and calculated intensity.

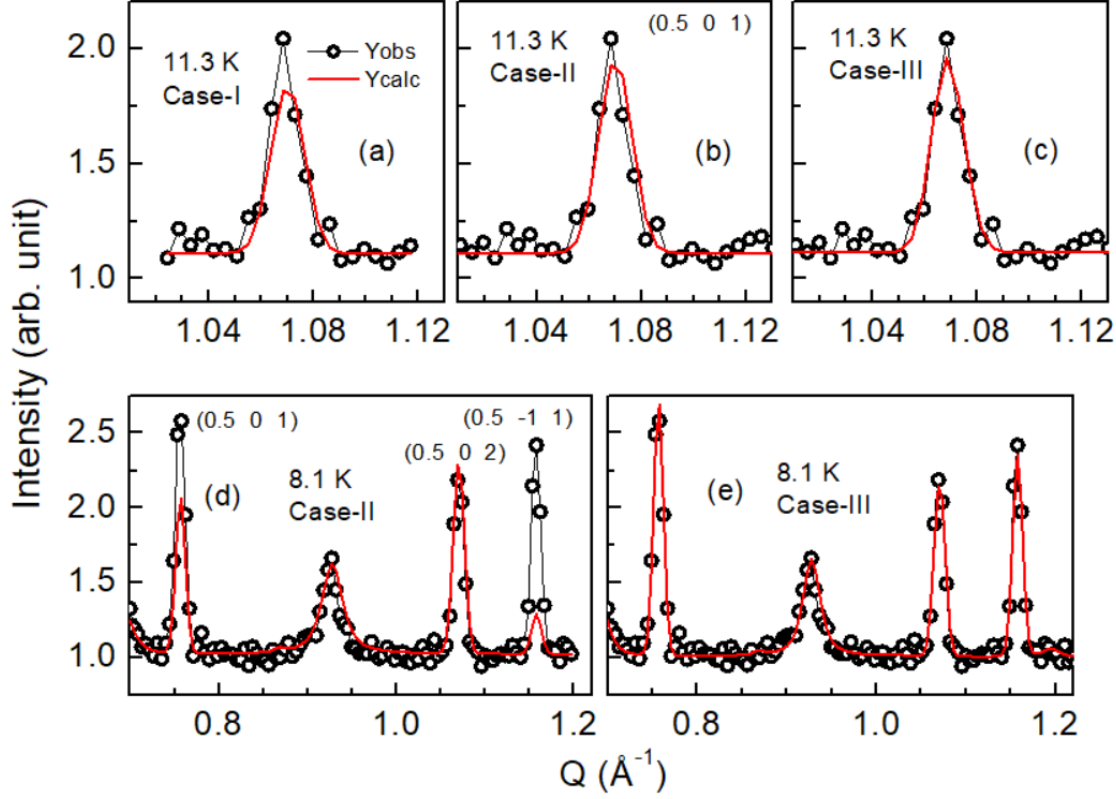


**Fig. 3:** Rietveld refinement at 11.3 K (a, b,c) and 8.1 K (d,e), as discussed in the text. Case-I: Refine only Ru-moment, keeping zero moment on Ho. Case-II: Fixing Ru-moment to its theoretical value/ what is obtained in case-I and refine the moment on Ho. Case-III: Refine moments on both Ru and Ho simultaneously

Below  $T_{N2}$ , we find that the propagation of the magnetic Bragg peaks can be well indexed for a combination of two different wave-vectors, which are,  $\mathbf{K}_1 = (0.5 \ 0 \ 0)$  with  $\Gamma_7$  and  $\mathbf{K}_2 = (0.25 \ 0.25 \ 0)$  with  $\Gamma_1$ , for both Ho and Ru-atom (Fig.2d for 8.1 K and Fig.S3 in SM<sup>32</sup> for 1.5 K). This infers that two different magnetic phases coexist below  $T_{N2}$ . The neutron peak-shape is modeled with a Thompson-Cox-Hastings pseudo-Voigt function in Fullprof program which is convolution of Lorentzian and Gaussian functions. The peak shape of the magnetic Bragg reflections associated with the  $\mathbf{K}_1$  vector is Gaussian (negligible Lorentzian part), whereas, the magnetic Bragg reflections associated with the  $\mathbf{K}_2$  vector has a small Lorentzian component, which implies that magnetic correlation length associated with the  $\mathbf{K}_2$  structure is shorter than that associated with the  $\mathbf{K}_1$  structure.

**Table-1:** The magnetic moment of Ru and Ho and its projection along different axis and angle.

$T$ (K)	$\mathbf{K}_1 = (0.5 \ 0 \ 0)$								Angle with c-axis ( $^\circ$ )	
	Ho-Moment ( $\mu_B$ )				Ru-Moment ( $\mu_B$ )					
	$M_a$	$M_b$	$M_c$	$M_{Ho}$	$M_a$	$M_b$	$M_c$	$M_{Ru}$	$\mathbf{M}_{Ho}$	$\mathbf{M}_{Ru}$
80	-	-	-	-	-	-	-	-		
30	1.197	0.599	-0.102	1.042	-0.289	-0.144	0.778	0.817	94.4	22.5
19	1.452	0.726	-0.484	1.347	-0.717	-0.359	1.262	1.406	106.6	32.4
11.3	1.544	0.772	-0.648	1.486	-0.761	-0.380	1.443	1.586	110.6	30.5
8.1	3.447	1.723	3.951	4.952	-0.510	-0.255	-0.281	0.524	44.3	116.3
1.5	4.089	2.044	4.665	5.856	-0.489	-0.245	-0.388	0.574	44.4	54.6
<b><math>\mathbf{K}_2 = (0.25 \ 0.25 \ 0)</math> <math>T &lt; T_{N2}</math></b>										
8.1	4.127	4.127	0	4.127	1.245	0.865	0	1.105	90	90
1.5	5.212	5.212	0	5.212	1.148	0.531	0	0.995	90	90

The magnetic structures associated with these two magnetic phases are depicted in Fig. 4. At  $T_{N2} < T < T_{N1}$ , for instance,  $T = 30$  K, both Ho and Ru spins are ordered ferromagnetically along the b-axis and antiferromagnetically in the ac-plane (AFM along the a-axis and canted AFM along the c-axis), as shown in Fig. 4(a). The Ho spins are nearly aligned in the ab-plane with a slight tilting towards the c-axis, whereas the Ru spins are nearly aligned along the c-axis with a tilting towards the ab-plane. With lowering the temperature, the magnetic structure remains nearly the same but with more tilting of both Ho and Ru moments towards the c-axis and an enhancement momentum size (Fig. 4b for 11.3 K and Table 1). This is indicative of strong  $4d$ - $4f$  magnetic correlation in this system. Below  $T_{N2}$ , there is a change in magnetic structure. Fig. 4 (c,d) represent the magnetic structures associated with  $\mathbf{K}_1 = (0.5 \ 0 \ 0)$  and  $\mathbf{K}_2 = (0.25 \ 0.25 \ 0)$  propagation wave vectors respectively by refining the neutron scattering data measured at  $T = 8.1$  K. As illustrated in Fig. 4(c), the magnetic structure associated with  $\mathbf{K}_1$  remains nearly the same below and above  $T_{N2}$ . Nevertheless, the component of Ho magnetic moment ( $M_c$ ) along the c-axis is significantly enhanced below  $T_{N2}$ , compared to the  $M_a$  and  $M_b$  components along a and b axes (see Table-1). In contrast,  $M_c$  of the Ru-magnetic moment is significantly reduced, compared to the  $M_a$  and  $M_b$  components, which is distinct from the scenario observed above  $T_{N2}$ . Interestingly, such spin reorientation of both Ho and Ru moments gives rise to the extinction of the  $(0.5 \ 0 \ 1)$  and  $(0.5 \ -1 \ 1)$  magnetic Bragg peaks above  $T_{N2}$  while the  $(0.5 \ 0 \ 2)$  magnetic Bragg peak persists. The calculated and experimentally obtained intensity of the magnetic peaks are listed in Table-2. Fig. 4 (d) shows the refined magnetic structure associated with  $\mathbf{K}_2$ . For this magnetic phase, both Ho and Ru spins are completely aligned in the ab-plane with an up-up-down-down antiferromagnetic structure, while spins are ferromagnetically aligned along the c-axis. Note that the total magnetic moment

of Ho-atom is nearly saturated ( $\sim 10.1 \mu_B$ ) at  $T = 8.1$  K, and the total magnetic moment of Ru is about  $1.6 \mu_B$ . The magnetic structure remains same down to  $T = 1.5$  K (Figure S4 and S5 in SM)<sup>32</sup>.

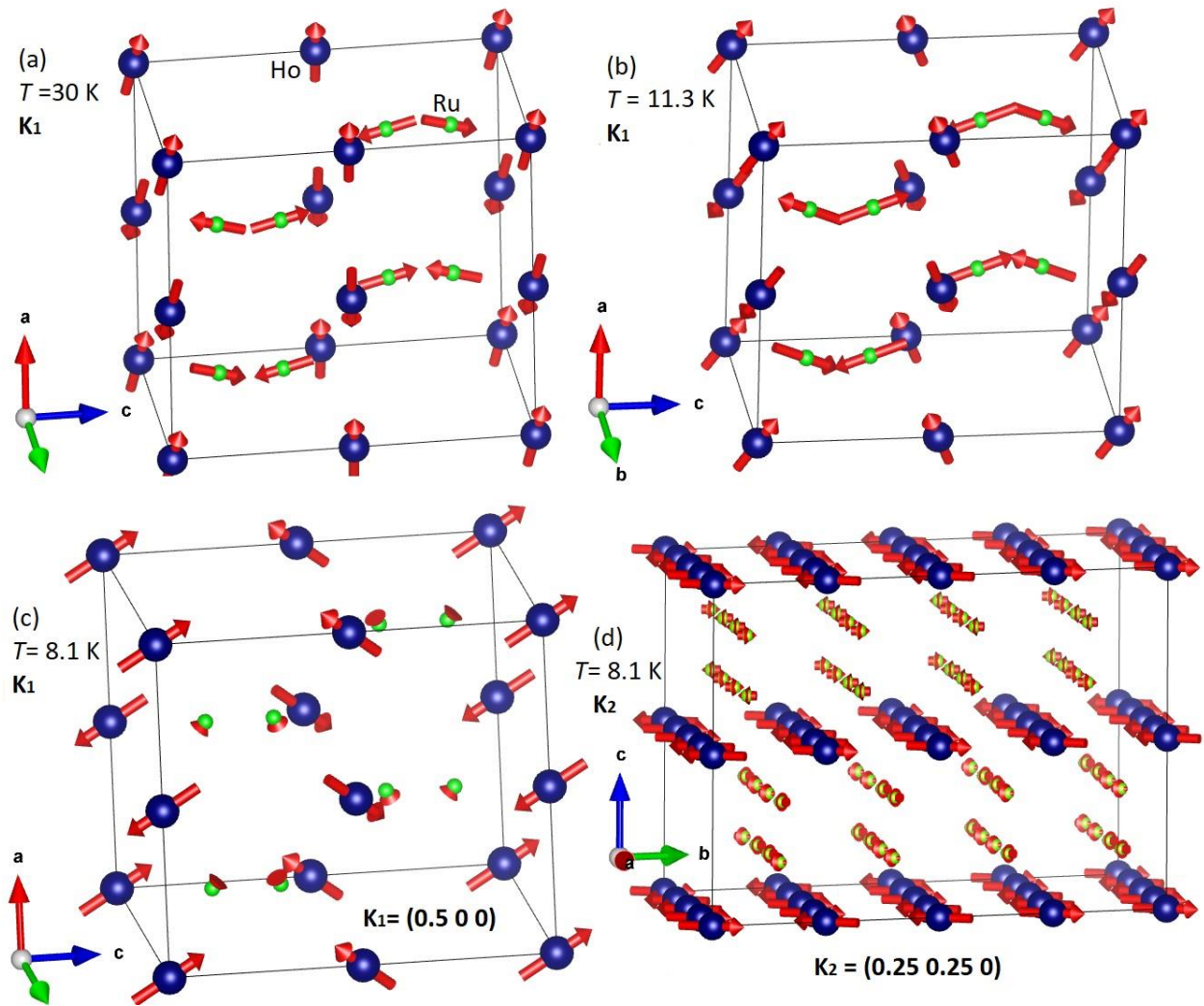


**Fig. 4:** (a) and (b) represent magnetic structure at  $T = 30$  K and  $11.3$  K, respectively. (c) and (d) represent magnetic structure at  $8.1$  K, associated with  $\mathbf{K}_1$  and  $\mathbf{K}_2$ , respectively. The length of magnetic vectors represents the relative moment size of Ho (blue) and Ru (green).

The observation of two magnetic orderings in Ba<sub>3</sub>HoRu<sub>2</sub>O<sub>9</sub> is quite intriguing. First, no anomaly indicating the existence of long-range ordering (LRO) at  $T_{N1}$  around  $50$  K is observed in both bulk magnetic susceptibility and heat capacity measurements presented in Fig. 1(a). This is presumably because the magnetic ordering at  $T_{N1}$  is weak in nature, where both Ho and Ru spins start to order but with small magnetic moment. Because of short-range magnetic correlation above  $T_{N1}$ , entropy starts to vary slowly from high temperature with lowering the temperature, crosses over with a minimal change around  $T_{N1}$  due to weak magnetic ordering, followed by further gradual

changes due to continuous slow spin-saturation and spin-reorientation with further lowering temperature. Despite the absence of anomaly in heat capacity at  $T_{N1}$ , one can clearly observe the onset of a bifurcation of heat capacity measured at zero and high magnetic field as shown in Fig. 1(a). Right below  $T_{N2}$  the Ho-moment quickly saturates and there is also a sharp spin-reorientation of Ho and Ru-moments, which gives rise to a maximum in the temperature dependent magnetic susceptibility and a large change in entropy leading to an anomaly in heat capacity. The absence of anomaly in magnetic susceptibility and heat capacity at the onset of magnetic ordering is unusual but not rare. Haldane spin-chain system ( $R_2\text{BaNiO}_5$ ) exhibits similar features,<sup>5</sup> where long-range magnetic ordering develops at high temperature as revealed by neutron diffraction measurement, but it does not yield an anomaly in magnetic susceptibility and heat capacity until spin-reorientation and spin-saturation occur at lower temperature. The Gaussian nature of the peak-shape of magnetic reflections associated with  $\mathbf{K}_1$  confirms the LRO below  $T_{N1}$ . In contrast, the Lorentzian part in the peak-shape of magnetic reflections associated with  $\mathbf{K}_2$  indicates a shorter magnetic correlation length. However,  $\lambda$ -shape anomaly in heat-capacity (Fig.1a) below  $T_{N2}$  is consistent with LRO as observed in a typical magnet. It is likely that the system forms finite-size magnetic domains instead of a perfect LRO below  $T_{N2}$  associated with  $\mathbf{K}_2$ . Such finite-size up-up-down-down magnetic domains instead of true LRO below  $T_{N2}$  have been predicted for the multiferroic compound  $\text{Ca}_3\text{CoMnO}_6$ , in which the small ferroelectric polarization compared to that of theoretical value is considered due to cancellations of polarization originating from different magnetic domains.<sup>33</sup> The small ferroelectric polarization for our titled compound at 5 K (see Ref.<sup>25</sup>) may be justified using same rationale if the ferroelectricity stems from the up-up-down-down spin-structure.

Second, Ho and Ru spins simultaneously develop long range ordering below  $T_{N1}$ . In general, rare-earth ions often order at relatively low temperature because of the weak magnetic correlation due to their localized  $f$  orbitals. For instance,  $\text{Ho}_2\text{Ru}_2\text{O}_7$  undergoes two magnetic phase transitions with Ru moment ordered at higher temperature ( $\sim 95$  K) followed by the ordering of Ho ions at lower temperature ( $\sim 1.4$  K) due to the enhanced internal magnetic field arising from the ordered Ru sublattice.<sup>8,9</sup> The concurrent ordering of Ho and Ru moment at 50 K in  $\text{Ba}_3\text{HoRu}_2\text{O}_9$  in the current study signals stronger Ho( $4f$ )-Ru( $4d$ ) magnetic correlation. Based on Goodenough-Anderson-Kanamori rules, the dominant nearest-neighbor exchange interactions in this system include i) strong  $179^\circ$  Ru-O-Ho antiferromagnetic super-exchange interaction (see crystal structure in Fig. S6 in SM)<sup>32</sup>, ii)  $-78^\circ$  Ru-O-Ho antiferromagnetic super-exchange interaction, and iii) weak Ru-Ru ferromagnetic direct exchange interaction (Ru-Ru of a dimer  $\sim 2.55$  Å which is less than Ru-Ru distance (2.65 Å) in a metal). The dominant  $179^\circ$  Ru-O-Ho antiferromagnetic super-exchange compared to Ru-O-Ru and Ru-Ru magnetic interaction in  $\text{Ba}_3\text{Ho}^{+3}\text{Ru}^{+4.5}_2\text{O}_9$  could be one possible reason of simultaneous magnetic ordering of Ru and Ho-ions compared to that of the  $\text{Ho}_2\text{Ru}_2\text{O}_7$  system (where Ho-O-Ru and Ru-O-Ru both exhibit  $\sim 109^\circ$  super-exchange interaction).<sup>9</sup> The light  $R$ -member  $\text{Ba}_3\text{NdRu}_2\text{O}_9$  in this family exhibits FM ordering below 24 K, followed by another magnetic ordering  $\sim 17$ -18 K. The Nd-moments align ferromagnetically below 24 K associated with a (0 0 0) wave vector and become canted antiferromagnetically ordered below 17 K with the same  $\mathbf{K}$ -vector, whereas  $\text{Ru}_2\text{O}_9$ -dimers order antiferromagnetically with a (0.5 0 0)

wave vector,<sup>20</sup> unlike this compound. The Ru-moments are canted in a Ru<sub>2</sub>O<sub>9</sub> dimer in the titled system, unlike FM arrangement of Ru-moments in intra-dimer in Ba<sub>3</sub>NdRu<sub>2</sub>O<sub>9</sub> compound,<sup>20</sup> and unlike the earlier prediction of AFM-dimer in this family for all *R*-members.<sup>17,28,29</sup>

**Table-2: Calculated and experimentally obtained intensity, obtained from riveted refinement in Fullprof Suite program, for particular peaks for different temperature.**

H K L	Associated k-vector	T (K)	I <sub>calc</sub>	I <sub>expt</sub>
<b>0.5 0 1</b>	<b>½ 0 0</b>	<b>1.5</b>	<b>374.6</b>	<b>383.8</b>
		<b>8.1</b>	<b>255.9</b>	<b>260.9</b>
		<b>11.3</b>	<b>11.4</b>	<b>5.1</b>
		<b>19</b>	<b>5.6</b>	<b>3.6</b>
		<b>30</b>	<b>1.4</b>	<b>0.0</b>
<b>0.5 0 2</b>		<b>1.5</b>	<b>121.6</b>	<b>131.1</b>
		<b>8.1</b>	<b>90.6</b>	<b>93.8</b>
		<b>11.3</b>	<b>96.0</b>	<b>114.8</b>
		<b>19</b>	<b>80.0</b>	<b>84.5</b>
		<b>30</b>	<b>38.5</b>	<b>40.5</b>
<b>0.5 -1 1</b>		<b>1.5</b>	<b>306.3</b>	<b>328.7</b>
		<b>8.1</b>	<b>210.7</b>	<b>217.8</b>
		<b>11.3</b>	<b>5.0</b>	<b>7.9</b>
		<b>19</b>	<b>5.0</b>	<b>1.1</b>
		<b>30</b>	<b>4.2</b>	<b>3.5</b>
<b>0.25 0.25 1</b>	<b>¼ ¼ 0</b>	<b>1.5</b>	<b>220.4</b>	<b>206.1</b>
<b>0.75 -0.25 1</b>		<b>8.1</b>	<b>141.3</b>	<b>132.2</b>
		<b>1.5</b>	<b>185.8</b>	<b>181.5</b>
		<b>8.1</b>	<b>114.8</b>	<b>113.1</b>

Third, two distinct magnetic phases coexist below  $T_{N2}$ , as illustrated in Fig. 4(b,c), one is associated with  $\mathbf{K}_1 = (0.5\ 0\ 0)$  and the other is associated with  $\mathbf{K}_2 = (0.25\ 0.25\ 0)$ . Each  $\mathbf{K}$  vector corresponds to magnetic ordering of both Ru and Ho simultaneously, unlike many other complex systems where two different  $\mathbf{K}$ -vectors are associated respectively with two different magnetic sublattices for different atoms or different crystallographic sites of the same atom.<sup>34-36</sup> Simultaneous ordering of both TM and *R* ions at high temperature is also reported in the multiferroic compounds RMn<sub>2</sub>O<sub>5</sub><sup>3,37-39</sup> and R<sub>2</sub>BaNiO<sub>5</sub><sup>4,5</sup>, which exhibit successive magnetic anomalies at lower temperature. However, no such magnetic phase coexistence was observed at a particular same *T*-regime for these oxides. Magnetic phase coexistence below metal-insulator transition temperature was observed in a layered ruthenate system, Fe-doped Ca<sub>3</sub>Ru<sub>2</sub>O<sub>7</sub>, where the

coexistence of commensurate and incommensurate phases arises from competing FM and AFM in-plane Ru-Ru interactions<sup>40</sup>. Note that the incommensurate phase stems from the commensurate one as a result of modification in the FM exchange interaction due to Fe doping. In contrast, here we demonstrate an unconventional magnetic phase coexistence in a magnetically three-dimensional compound,  $\text{Ba}_3\text{HoRu}_2\text{O}_9$ , where two coexisting magnetic phases are completely different and the phase competition arises as a result of different competing exchange interactions. It is likely that the Ho-O-Ru super-exchange interaction starts to dominate below  $T_{N2}$  and Ru-moments align with stronger Ho-moments, which results in spin-reorientation and the emergence of another spin configuration within the ab-plane by minimizing the exchange frustration. However, other parameters, such as crystal-field effect, magnetic anisotropy, may play a role as well, which needs further theoretical/spectroscopic investigations. An external parameter, like magnetic field or pressure, may stabilize to a particular magnetic phase by tuning the competing interactions.

In summary, we have revisited magnetic properties of multiferroic compound  $\text{Ba}_3\text{HoRu}_2\text{O}_9$  via comprehensive neutron powder diffraction measurements. We find that this material undergoes two magnetic phase transitions, instead of one, at  $T_{M1} \approx 50$  K and  $T_{N2} \approx 10$  K, where both Ho and Ru spins develop long range order simultaneously. This suggests a strong  $4d$  (Ru)- $4f$  (Ho) magnetic correlation. In addition, below  $T_{N2}$  we unravel a coexistence of two magnetic phases associated with completely two different propagation wave vectors, implying competition among different exchange interactions. This study demonstrates that  $\text{Ba}_3\text{RRu}_2\text{O}_9$  system provides a unique platform to study the cooperative  $3d$ - $4f$  phenomena where Ru and  $R$  moments are strongly coupled and compete with other exchange interactions. Our new interesting results further call for reinvestigation of magnetic orderings in other  $R$ -Ru based systems in general. The up-up-down-down structure could be the possible reason for observation of polarization below  $T_{N2}$ . A detail investigation on electric polarization for this compound will be published elsewhere.

Work at Michigan State University was supported by the U.S. Department of Energy, Office of Science, Office of Basic Energy Sciences, Materials Sciences and Engineering Division under Award No. DE-SC0019259.

## References:

- <sup>1</sup> Y. Tokura, S. Seki, and N. Nagaosa, Reports on Progress in Physics **77**, 076501 (2014).
- <sup>2</sup> S.H. Kang, H.J. Lee, I.W. Kim, T.H. Jang, Y.H. Jeong, and T.Y. Koo, Journal of the Korean Physical Society **51**, 669 (2007).
- <sup>3</sup> N. Hur, S. Park, P.A. Sharma, J.S. Ahn, S. Guha, and S.-W. Cheong, Nature **429**, 392 (2004).
- <sup>4</sup> K. Singh, T. Basu, S. Chowki, N. Mahapatra, K.K. Iyer, P.L. Paulose, and E.V. Sampathkumaran, Physical Review B **88**, 094438 (2013).
- <sup>5</sup> E. García-Matres, J.L. Martínez, and J. Rodríguez-Carvajal, Eur. Phys. J. B **24**, 59 (2001).
- <sup>6</sup> J.G. Rau, E.K.-H. Lee, and H.-Y. Kee, Annual Review of Condensed Matter Physics **7**, 195 (2016).

- <sup>7</sup> J.T. Rijssenbeek, P. Matl, B. Batlogg, N.P. Ong, and R.J. Cava, *Phys. Rev. B* **58**, 10315 (1998).
- <sup>8</sup> N. Taira, M. Wakeshima, and Y. Hinatsu, *J. Phys.: Condens. Matter* **11**, 6983 (1999).
- <sup>9</sup> C.R. Wiebe, J.S. Gardner, S.-J. Kim, G.M. Luke, A.S. Wills, B.D. Gaulin, J.E. Greedan, I. Swainson, Y. Qiu, and C.Y. Jones, *Phys. Rev. Lett.* **93**, 076403 (2004).
- <sup>10</sup> S.T. Ku, D. Kumar, M.R. Lees, W.-T. Lee, R. Aldus, A. Studer, P. Imperia, S. Asai, T. Masuda, S.W. Chen, J.M. Chen, and L.J. Chang, *J. Phys.: Condens. Matter* **30**, 155601 (2018).
- <sup>11</sup> N. Taira, M. Wakeshima, Y. Hinatsu, A. Tobo, and K. Ohoyama, *Journal of Solid State Chemistry* **176**, 165 (2003).
- <sup>12</sup> J.S. Gardner and G. Ehlers, *J. Phys.: Condens. Matter* **21**, 436004 (2009).
- <sup>13</sup> X.A. Velásquez Moya, R. Cardona, J.I. Villa Hernández, D.A. Landínez Téllez, and J. Roa-Rojas, *Journal of Electronic Materials* **47**, 3421 (2018).
- <sup>14</sup> Y. Hinatsu, Y. Izumiyama, Y. Doi, A. Alemi, M. Wakeshima, A. Nakamura, and Y. Morii, *Journal of Solid State Chemistry* **177**, 38 (2004).
- <sup>15</sup> Y. Izumiyama, Y. Doi, M. Wakeshima, Y. Hinatsu, K. Oikawa, Y. Shimojo, and Y. Morii, *J. Mater. Chem.* **10**, 2364 (2000).
- <sup>16</sup> Y. Shimoda, Y. Doi, M. Wakeshima, and Y. Hinatsu, *Journal of Solid State Chemistry* **183**, 33 (2010).
- <sup>17</sup> Y. Doi, M. Wakeshima, Y. Hinatsu, A. Tobo, K. Ohoyama, and Y. Yamaguchi, *J. Mater. Chem.* **11**, 3135 (2001).
- <sup>18</sup> Y. Doi and Y. Hinatsu, *Journal of Solid State Chemistry* **177**, 3239 (2004).
- <sup>19</sup> W. Müller, M. Avdeev, Q. Zhou, A.J. Studer, B.J. Kennedy, G.J. Kearley, and C.D. Ling, *Phys. Rev. B* **84**, 220406 (2011).
- <sup>20</sup> M.S. Senn, S.A.J. Kimber, A.M. Arevalo Lopez, A.H. Hill, and J.P. Attfield, *Phys. Rev. B* **87**, 134402 (2013).
- <sup>21</sup> T. Susuki, N. Kurita, T. Tanaka, H. Nojiri, A. Matsuo, K. Kindo, and H. Tanaka, *Phys. Rev. Lett.* **110**, 267201 (2013).
- <sup>22</sup> H.D. Zhou, E.S. Choi, G. Li, L. Balicas, C.R. Wiebe, Y. Qiu, J.R.D. Copley, and J.S. Gardner, *Phys. Rev. Lett.* **106**, 147204 (2011).
- <sup>23</sup> S.A.J. Kimber, M.S. Senn, S. Fratini, H. Wu, A.H. Hill, P. Manuel, J.P. Attfield, D.N. Argyriou, and Paul.F. Henry, *Phys. Rev. Lett.* **108**, 217205 (2012).
- <sup>24</sup> J. Hwang, E.S. Choi, F. Ye, C.R. Dela Cruz, Y. Xin, H.D. Zhou, and P. Schlottmann, *Phys. Rev. Lett.* **109**, 257205 (2012).
- <sup>25</sup> T. Basu, V. Caignaert, S. Ghara, X. Ke, A. Pautrat, S. Krohns, A. Loidl, and B. Raveau, *Phys. Rev. Mater.* **3**, 114401 (2019).
- <sup>26</sup> C.D. Ling, Z. Huang, B.J. Kennedy, S. Rols, M.R. Johnson, M. Zbiri, S.A.J. Kimber, J. Hudspeth, D.T. Adroja, K.C. Rule, M. Avdeev, and P.E.R. Blanchard, *Phys. Rev. B* **94**, 174401 (2016).
- <sup>27</sup> T. Basu, A. Pautrat, V. Hardy, A. Loidl, and S. Krohns, *Appl. Phys. Lett.* **113**, 042902 (2018).
- <sup>28</sup> Y. Doi, Y. Hinatsu, Y. Shimojo, and Y. Ishii, *Journal of Solid State Chemistry* **161**, 113 (2001).
- <sup>29</sup> Y. Doi and Y. Hinatsu, *J. Mater. Chem.* **12**, 1792 (2002).
- <sup>30</sup> J. Rodríguez-Carvajal, *Physica B: Condensed Matter* **192**, 55 (1993).
- <sup>31</sup> A.S. Wills, *Physica B: Condensed Matter* **276–278**, 680 (2000).
- <sup>32</sup>(n.d.).
- <sup>33</sup> Y.J. Choi, H.T. Yi, S. Lee, Q. Huang, V. Kiryukhin, and S.-W. Cheong, *Physical Review Letters* **100**, 047601 (2008).
- <sup>34</sup> B. Prévost, N. Gauthier, V.Y. Pomjakushin, B. Delley, H.C. Walker, M. Kenzelmann, and A.D. Bianchi, *Phys. Rev. B* **98**, 144428 (2018).
- <sup>35</sup> Y. Zhao, J.W. Lynn, G.S. Thakur, Z. Haque, L.C. Gupta, and A.K. Ganguli, *Journal of Physics and Chemistry of Solids* **111**, 1 (2017).
- <sup>36</sup> J. Rodríguez-Carvajal and J. Villain, *Comptes Rendus Physique* **20**, 770 (2019).

<sup>37</sup> S.H. Bukhari, T. Kain, M. Schiebl, A. Shuvaev, A. Pimenov, A.M. Kuzmenko, X. Wang, S.-W. Cheong, J. Ahmad, and A. Pimenov, *Physical Review B* **94**, 174446 (2016).

<sup>38</sup> N. Hur, S. Park, P.A. Sharma, S. Guha, and S.-W. Cheong, *Phys. Rev. Lett.* **93**, 107207 (2004).

<sup>39</sup> S. Chattopadhyay, V. Balédent, F. Damay, A. Gukasov, E. Moshopoulou, P. Auban-Senzier, C. Pasquier, G. André, F. Porcher, E. Elkaim, C. Doubrovsky, M. Greenblatt, and P. Foury-Leylekian, *Phys. Rev. B* **93**, 104406 (2016).

<sup>40</sup> X. Ke, J. Peng, W. Tian, T. Hong, M. Zhu, and Z.Q. Mao, *Phys. Rev. B* **89**, 220407 (2014).

### Supplemental Material

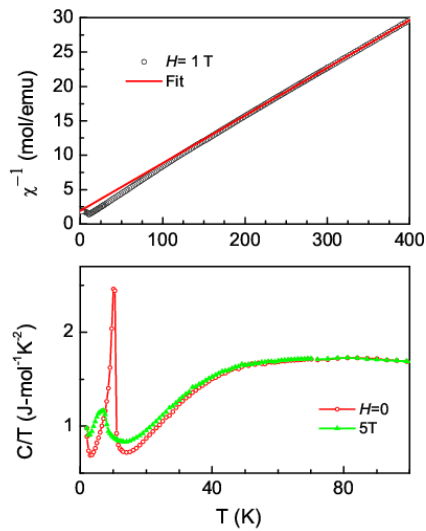


**Fig. S1:** (a) Inverse magnetic susceptibility as a function of temperature in presence of 1 T magnetic field from 2-320 K. The solid red line is a linear fit. (b) Heat Capacity divided by temperature as a function of temperature for zero magnetic field.

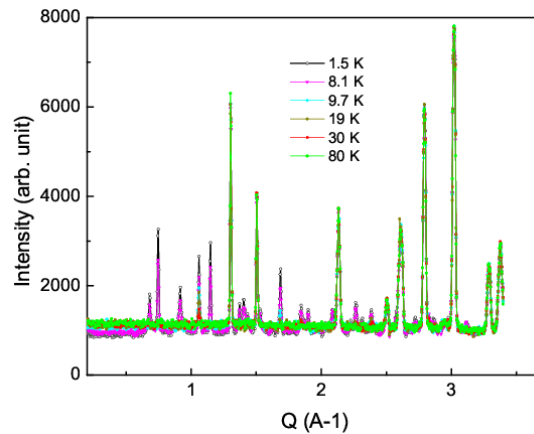


**Fig. S2:** Neutron diffraction intensity at several ferretures for large Q-range to get a better view of no change of magnetic intensity at nuclear Bragg peaks.

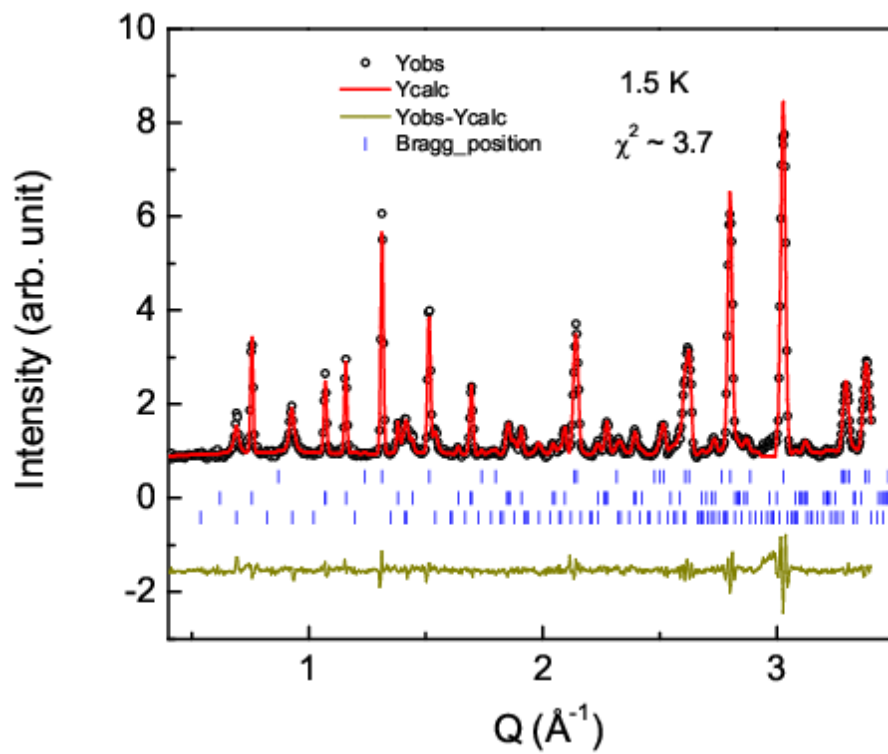


**Fig. S3:** Rietveld refinement at 1.5 K

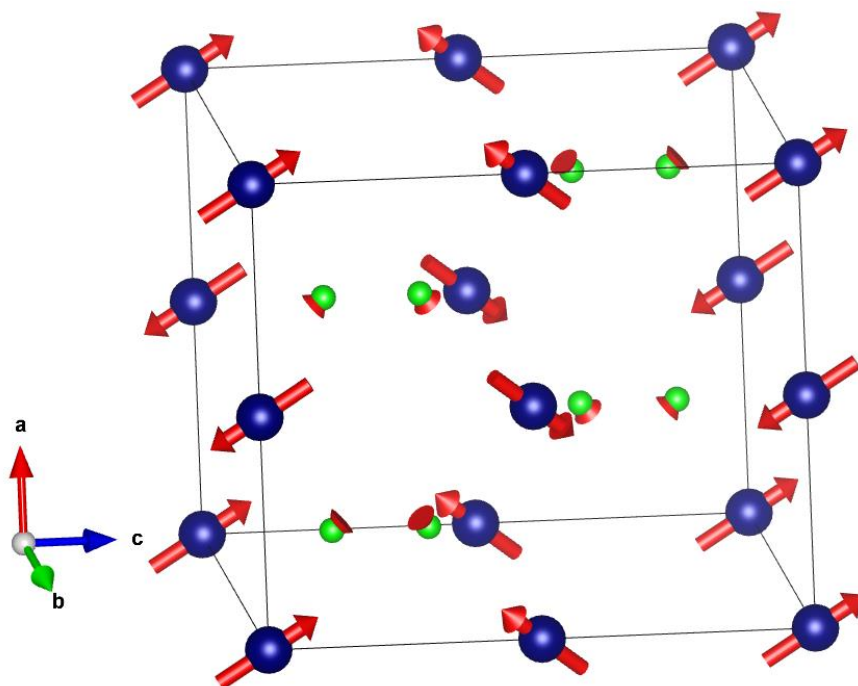


**Fig. S4:** Magnetic structure at 1.5 K associated with  $k = \frac{1}{2} 0 0$ .

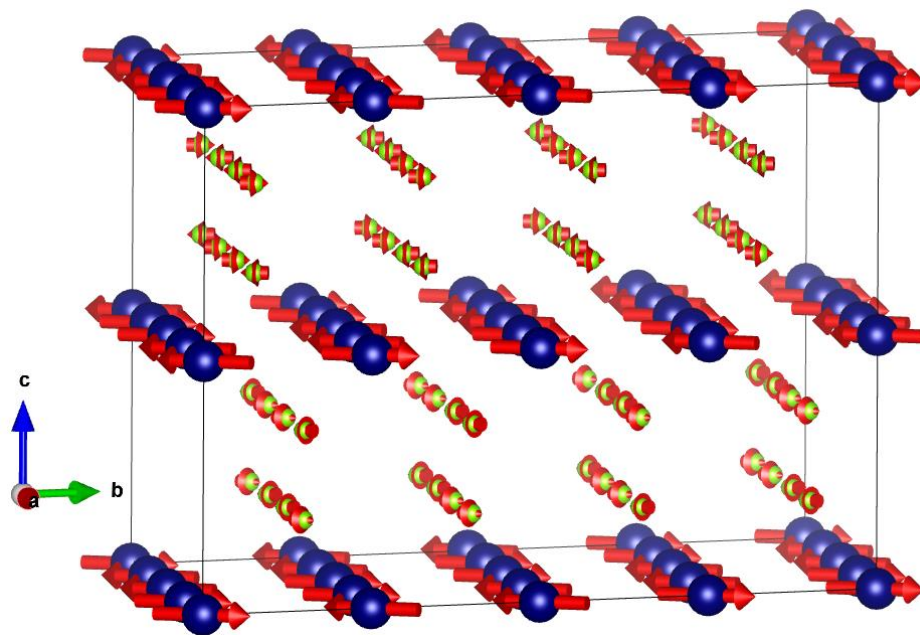
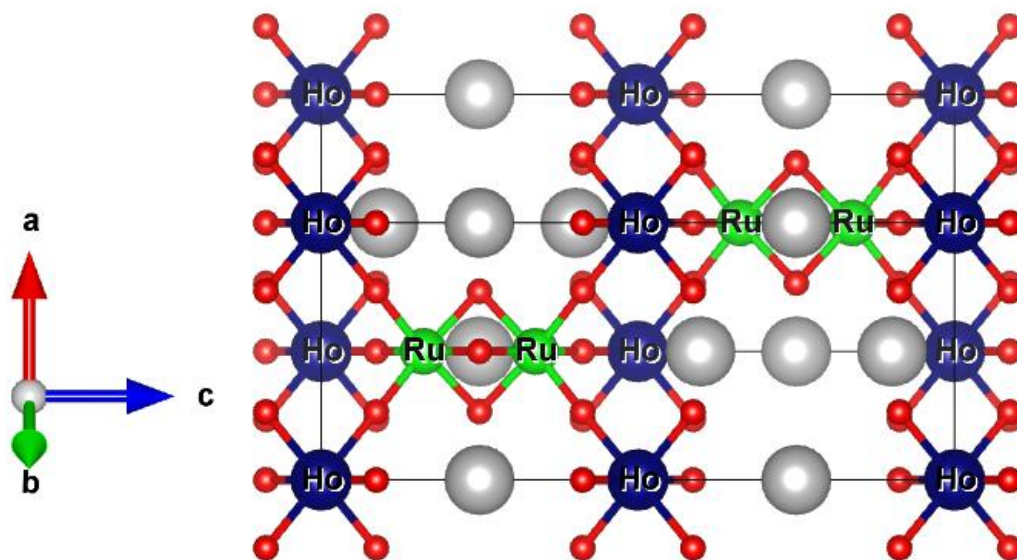


Fig. S5: Magnetic structure at 1.5 K associated with  $k=\frac{1}{4} \frac{1}{4} 0$



Figures S6: Crystal structure of  $\text{Ba}_3\text{HoRu}_2\text{O}_9$ .

**Table-S1: Allowed k-vector for space group P63/mmc.**

k-vector description		ITA description	
k-vector label	Conventional basis	Wyckoff position	
		Multiplicity	Letter
<b>GM</b>	0,0,0	1	a
<b>A</b>	0,0,1/2	1	b
<b>K</b>	1/3,1/3,0	2	c
<b>H</b>	1/3,1/3,1/2	2	d
<b>DT</b>	0,0,u	2	e
<b>M</b>	1/2,0,0	3	f
<b>L</b>	1/2,0,1/2	3	g
<b>P</b>	1/3,1/3,u	4	h
<b>U</b>	1/2,0,u	6	i
<b>SM</b>	u,0,0	6	j
<b>R</b>	u,0,1/2	6	k
<b>LD (T)</b>	u,u,0	6	l
<b>Q (S)</b>	u,u,1/2	6	m
<b>D</b>	u,0,v	12	n
<b>C (F)</b>	u,u,v	12	o
<b>B</b>	u,v,0	12	p
<b>E</b>	u,v,1/2	12	q
<b>GP</b>	u,v,w	24	r

**Table-S2: Basis vector for the space group P63/mmc for  $k=0.5 \ 0 \ 0$ . The irreducible representation for magnetic site Ru (0.66667 0.33333 0.16164), as obtained from SARAh program.**

IR	BV	Atom	BV components					
			$m_{\parallel a}$	$m_{\parallel b}$	$m_{\parallel c}$	$im_{\parallel a}$	$im_{\parallel b}$	$im_{\parallel c}$
$\Gamma_1$	$\psi_1$	1	0	-1	0	0	0	0
		2	0	-1	0	0	0	0
		3	0	1	0	0	0	0
		4	0	1	0	0	0	0
$\Gamma_2$	$\psi_2$	1	2	1	0	0	0	0
		2	2	1	0	0	0	0
		3	2	1	0	0	0	0
		4	2	1	0	0	0	0
	$\psi_3$	1	0	0	2	0	0	0
		2	0	0	-2	0	0	0
		3	0	0	2	0	0	0
		4	0	0	-2	0	0	0
$\Gamma_3$	$\psi_4$	1	2	1	0	0	0	0
		2	2	1	0	0	0	0
		3	-2	-1	0	0	0	0
		4	-2	-1	0	0	0	0
	$\psi_5$	1	0	0	2	0	0	0
		2	0	0	-2	0	0	0
		3	0	0	-2	0	0	0
		4	0	0	2	0	0	0
$\Gamma_4$	$\psi_6$	1	0	-1	0	0	0	0
		2	0	-1	0	0	0	0
		3	0	-1	0	0	0	0
		4	0	-1	0	0	0	0
$\Gamma_5$	$\psi_7$	1	0	-1	0	0	0	0
		2	0	1	0	0	0	0
		3	0	1	0	0	0	0
		4	0	-1	0	0	0	0
$\Gamma_6$	$\psi_8$	1	2	1	0	0	0	0
		2	-2	-1	0	0	0	0
		3	2	1	0	0	0	0
		4	-2	-1	0	0	0	0
	$\psi_9$	1	0	0	2	0	0	0
		2	0	0	2	0	0	0
		3	0	0	2	0	0	0
		4	0	0	2	0	0	0
$\Gamma_7$	$\psi_{10}$	1	2	1	0	0	0	0
		2	-2	-1	0	0	0	0
		3	-2	-1	0	0	0	0
		4	2	1	0	0	0	0

IR	BV	Atom	BV components					
			$m_a$	$m_b$	$m_c$	$im_a$	$im_b$	$im_c$
$\Gamma_8$	$\psi_{11}$	1	0	0	2	0	0	0
		2	0	0	2	0	0	0
		3	0	0	-2	0	0	0
		4	0	0	-2	0	0	0
	$\psi_{12}$	1	0	-1	0	0	0	0
		2	0	1	0	0	0	0
		3	0	-1	0	0	0	0
		4	0	1	0	0	0	0

**Table-S3: Basis vector for the space group P63/mmc for  $k=0.5 \ 0 \ 0$ . The irreducible representation for magnetic site Ho ( $0 \ 0 \ 0$ ), as obtained from SARAh program.**

IR	BV	Atom	BV components					
			$m_{\parallel a}$	$m_{\parallel b}$	$m_{\parallel c}$	$im_{\parallel a}$	$im_{\parallel b}$	$im_{\parallel c}$
$\Gamma_1$	$\psi_1$	1	0	-2	0	0	0	0
		2	0	2	0	0	0	0
$\Gamma_3$	$\psi_2$	1	4	2	0	0	0	0
		2	-4	-2	0	0	0	0
	$\psi_3$	1	0	0	4	0	0	0
		2	0	0	4	0	0	0
$\Gamma_5$	$\psi_4$	1	0	-2	0	0	0	0
		2	0	-2	0	0	0	0
$\Gamma_7$	$\psi_5$	1	4	2	0	0	0	0
		2	4	2	0	0	0	0
	$\psi_6$	1	0	0	4	0	0	0
		2	0	0	-4	0	0	0

**Table-S4: Basis vector for the space group P63/mmc for  $k=0.25\ 0.25\ 0$ . The irreducible representation for magnetic site Ru (0.66667 0.33333 0.16164), as obtained from SARAh program.**

IR	BV	Atom	BV components					
			$m_{\parallel a}$	$m_{\parallel b}$	$m_{\parallel c}$	$im_{\parallel a}$	$im_{\parallel b}$	$im_{\parallel c}$
$\Gamma_1$	$\psi_1$	1	1	0	0	0	0	0
		2	0	1	0	0	0	0
		3	-1	0	0	0	0	0
		4	0	-1	0	0	0	0
	$\psi_2$	1	0	1	0	0	0	0
		2	1	0	0	0	0	0
		3	0	-1	0	0	0	0
		4	-1	0	0	0	0	0
	$\psi_3$	1	0	0	1	0	0	0
		2	0	0	-1	0	0	0
		3	0	0	1	0	0	0
		4	0	0	-1	0	0	0
$\Gamma_2$	$\psi_4$	1	1	0	0	0	0	0
		2	0	1	0	0	0	0
		3	1	0	0	0	0	0
		4	0	1	0	0	0	0
	$\psi_5$	1	0	1	0	0	0	0
		2	1	0	0	0	0	0
		3	0	1	0	0	0	0
		4	1	0	0	0	0	0
	$\psi_6$	1	0	0	1	0	0	0
		2	0	0	-1	0	0	0
		3	0	0	-1	0	0	0
		4	0	0	1	0	0	0
$\Gamma_3$	$\psi_7$	1	1	0	0	0	0	0
		2	0	-1	0	0	0	0
		3	-1	0	0	0	0	0
		4	0	1	0	0	0	0
	$\psi_8$	1	0	1	0	0	0	0
		2	-1	0	0	0	0	0
		3	0	-1	0	0	0	0
		4	1	0	0	0	0	0
	$\psi_9$	1	0	0	1	0	0	0
		2	0	0	1	0	0	0
		3	0	0	1	0	0	0
		4	0	0	1	0	0	0
$\Gamma_4$	$\psi_{10}$	1	1	0	0	0	0	0
		2	0	-1	0	0	0	0
		3	1	0	0	0	0	0
		4	0	-1	0	0	0	0

IR	BV	Atom	BV components					
			$m_a$	$m_b$	$m_c$	$im_a$	$im_b$	$im_c$
$\psi_{11}$		1	0	1	0	0	0	0
		2	-1	0	0	0	0	0
		3	0	1	0	0	0	0
		4	-1	0	0	0	0	0
$\psi_{12}$		1	0	0	1	0	0	0
		2	0	0	1	0	0	0
		3	0	0	-1	0	0	0
		4	0	0	-1	0	0	0

**Table-S5: Basis vector for the space group P63/mmc for  $\mathbf{k}=.25\ 0.25\ 0$ . The irreducible representation for magnetic site Ho (0 0 0), as obtained from SARAh program.**

IR	BV	Atom	BV components					
			$m_{\parallel a}$	$m_{\parallel b}$	$m_{\parallel c}$	$im_{\parallel a}$	$im_{\parallel b}$	$im_{\parallel c}$
$\Gamma_1$	$\psi_1$	1	1	1	0	0	0	0
		2	-1	-1	0	0	0	0
$\Gamma_2$	$\psi_2$	1	1	1	0	0	0	0
		2	1	1	0	0	0	0
$\Gamma_3$	$\psi_3$	1	1	-1	0	0	0	0
		2	-1	1	0	0	0	0
$\Gamma_4$	$\psi_4$	1	0	0	2	0	0	0
		2	0	0	2	0	0	0
	$\psi_5$	1	1	-1	0	0	0	0
		2	1	-1	0	0	0	0
$\psi_6$	1	0	0	2	0	0	0	
	2	0	0	-2	0	0	0	